

# Identification of Material Properties under Strain-Controlled Non-Proportional Cyclic Loading

Z. L. Kowalewski

*In most cases of non-proportional cyclic loading, the investigated materials show additional hardening in comparison to the hardening observed under proportional loading path. For some materials, however, an opposite effect is observed. In the present paper, the above mentioned phenomena are experimentally investigated under non-proportional cyclic loading in form of circular path in a strain space and proportional cyclic loading (tension-compression) for three different commercial materials, i.e., brass, steel, and an aluminium alloy. An evolution of the mechanical properties due to cyclic loading is assessed using the concept of the yield surface determined in the two-dimensional stress space ( $\sigma$ ,  $\tau$ ). Effects of strain rate and magnitude of cyclic loading amplitude are also investigated. Analysis of the stress and strain signals during non-proportional cyclic loading has shown significant effect of a phase shift of the maximum stress with respect to the corresponding maximum strain, which was not observed during tests carried out along proportional loading paths.*

## 1 Introduction

Mechanical behaviour of structural materials under non-proportional loading has been investigated in many research centres, e.g. Lamba and Sidebottom (1978), Ohashi et al. (1985), Benallal and Marquis (1987), Khan and Wang (1988), Krempl and Lu (1984), Cheng and Krempl (1991), Krempl and Cheng (1993). Therefore, it is well known that the cyclic loading of metals along non-proportional paths may have more significant influence on material behaviour than that usually observed for proportional ones. Previous results achieved for different materials tested under non-proportional cyclic loading showed additional hardening in comparison to the hardening observed under proportional loading path, e.g. Murakami et al. (1989a), Murakami et al. (1989b), Calloch and Marquis (1997). It is usually assumed that such effect is due to a higher number of slip systems activated by the complex non-proportional loading, (Doong and Socie, 1991; Cailletaud et al., 1991).

Ohashi et al. (1985) carried out the tests investigating the cyclic stress-strain relations on 316 stainless steel for the tension - compression cycle and the circular cycle at 873 K under total stress control. The cyclic strain hardening was observed as a decrease in plastic strain amplitude. A salient non-proportional cyclic hardening along the circular path is manifested in contrast to the proportional cyclic strain hardening along a uni-axial tension - compression path realised for the control signal in form of sinusoid, i.e. the same as that used in the non-proportional cycling along circular path. Proportional tension-compression cycling was also carried out using control parameter in forms of triangle and trapezoid. As is shown in Figure 1a, there are not marked differences between the results for the same type of cycles achieved for three shapes of control parameter. The same material has also been investigated by Murakami et al. (1989) under non-proportional loading along a circular path and a uni-axial tension-compression, Figure 1b. In this case, however, all tests were total strain controlled. Besides of additional hardening of the material observed in comparison of the data for proportional and non-proportional loadings, the results show that the increase in stress amplitude, that is the cyclic strain hardening, rapidly develops at the early stage of inelastic strain accumulation and then it develops asymptotically to a state of constant stress amplitude (a saturated stress state).

From previous experimental works it is also known that for a certain class of materials the softening effect can be observed under non-proportional cyclic loadings, (Lamba and Sidebottom, 1978; Dietrich et al., 2000). Such difference between material behaviour under cyclic loading leads to the essential difficulties in the constitutive modelling. Therefore, for the rational formulation of a multiaxial cyclic constitutive equation, it is necessary to study a series of representative non-proportional cyclic behaviour, and to identify the property of the multiaxial cyclic hardening/or softening mechanisms. An interesting theoretical approach describing the effects mentioned above has been proposed by Tanaka (1994). In order to describe the behaviour of cyclic hardening and softening under proportional and non-proportional loading conditions, a certain form of a structural tensor was introduced

and a new non-proportionality factor has been defined. By introduction of two internal variables also the amplitude dependence of the cyclic hardening and softening has been taken into account in the model. In the present paper, the above-mentioned hardening/softening phenomenon is experimentally investigated under non-proportional cyclic loading (loading in form of circular path in a strain space) in complex stress states conditions for thin-walled tubular specimens using a tension-torsion hydraulic servo-controlled testing machine.

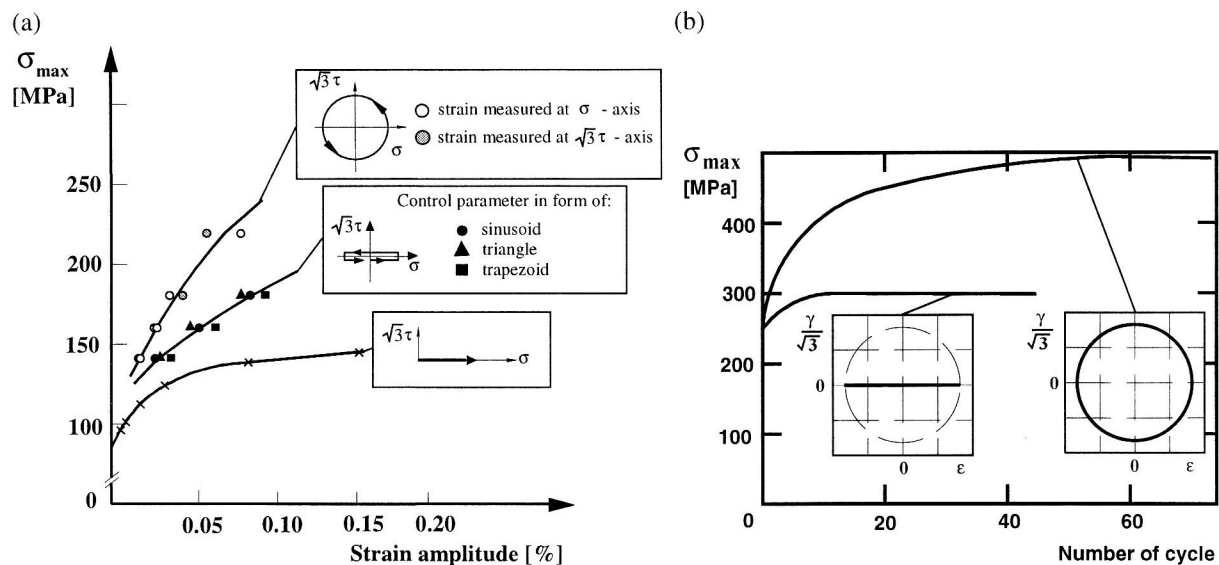


Figure 1. Experimental Data for 316 Stainless Steel: (a) Relation between Stress Amplitude and Accumulated Inelastic Strain for the Stress Controlled Tests (Ohashi et al., 1985), (b) Cyclic Stress-Strain Relations at 873 K under Tension-Compression Cycle and Circular Cycle (Murakami et al., 1989), Cycles Carried Out under Total Strain Amplitude Equal to 0.4%

## 2 Main Details of the Experimental Technique

Three different commercial materials were tested, i.e. MO58 brass, 55 steel, and PA6 aluminium alloy. The tubular thin-walled specimens were machined from extruded rods in the case of aluminium alloy and brass, whereas for the steel rolled rods were applied. All tests were carried out in the plane stress state produced within thin wall of the tubular specimen by the application of an axial force and torque using the hydraulic servo-controlled testing machine. Axial, shear, and hoop strains were measured using the strain gages bonded to the outer surface of the specimen and located near the terminal with strain gages wired to form three temperature compensated bridge circuits corresponding to the appropriate strain components.

## 3 Experimental Procedure

Non-proportional cyclic loading of all materials tested was total strain-controlled and variations of axial and shear strains were programmed to form a circle in the  $(\epsilon, \gamma/\sqrt{3})$  plane. During all cycles of loading all the strains were recorded in a digital form together with an axial force and torque. On the base of such data, and the specimen dimensions, the axial and shear stresses were calculated to observe a response of the material to the programme of deformation. For each material an analysis of the variations of the mechanical properties due to cyclic loading is based on the concept of a yield surface determined in the two-dimensional stress space  $(\sigma, \tau)$ . Yield surfaces were determined in the sequential mode (Kowalewski and Śliwowski, 1997; Kowalewski, 1997; Dietrich and Kowalewski, 1997); effective plastic strain 0.005% was introduced to the material during each probe of the yield surface determination procedure. Differences in programmes for all materials considered are connected with the variations of parameters of cyclic loading such as amplitudes, frequencies of cyclic loading, number of cycles, types of cyclic loading (proportional, non-proportional).

In the case of brass only one frequency (0.01Hz) of cyclic loading and one strain amplitude (0.65%) is taken into account. The procedure for this material comprised the determination of an initial yield surface, non-proportional cyclic loading (20 full cycles) and of a subsequent yield surface. The experimental programme for both

remaining materials is almost the same and comprised two essential parts: the uniaxial tension-compression cycles and the combined tension-torsion cycles along the circular path, Figure 2. In the first part after the determination of an initial yield locus, the proportional cyclic loading is applied for the selected strain amplitude. The main aim of this programme is to check whether the retardation time between maximum strain and maximum stress can be observed in the cycles of this type. Additionally, subsequent yield surfaces are determined for both materials in order to evaluate an influence of proportional cyclic loading on evolution of the initial yield locus. The second part of the experimental programme contained the following steps:

- initial yield surface determination,
- circular cycling with strain amplitude 0.0015 (10 cycles),
- second yield surface determination,
- circular cycling with strain amplitude 0.003 (10 cycles),
- third yield surface determination,
- circular cycling with strain amplitude 0.0065 (10 or 20 cycles),
- fourth yield surface determination.

The above testing programme has been performed for three frequencies of cycling: 0.0025Hz, 0.025Hz and 0.25Hz. The only difference between the programme for steel and aluminium alloy is connected with the number of cycles for the highest strain amplitude under the question (10 cycles for steel and 20 cycles for aluminium alloy). All tests have been performed at the room temperature.

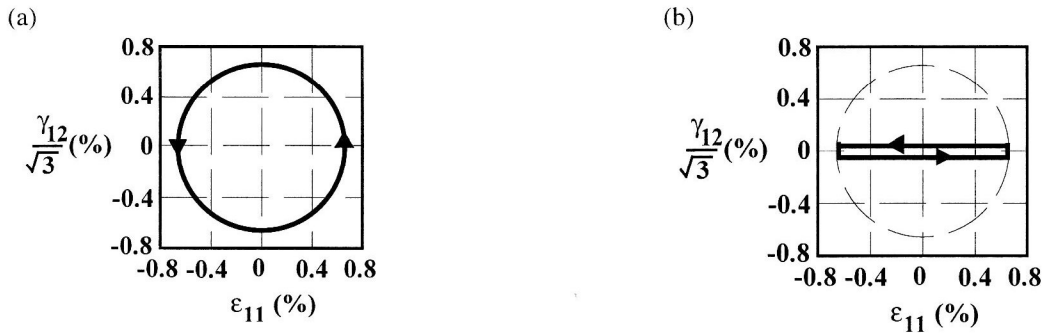


Figure 2. Cyclic Total-Strain Paths: (a) Circular Cycle, (b) Tension-Compression Cycle

### 3.1 Notations of the Equivalent Stress and Equivalent Strain

Stress and strain states are characterised by the Huber-Mises effective stress, and the Huber-Mises effective total strain. Thus, the biaxial stress and strain states applied on a thin-walled tubular specimens can be described using the following expressions

$$\sigma_{eq} = (\sigma^2 + 3\tau^2)^{1/2} \quad (1)$$

$$\varepsilon_{eq} = (\varepsilon^2 + \gamma^2/3)^{1/2} \quad (2)$$

where  $\sigma$ ,  $\tau$  are axial and shear stresses, respectively, while  $\varepsilon$ ,  $\gamma/2$  are total axial and total shear strains. The stress amplitudes and the strain amplitudes are defined as follows

$$\frac{\Delta\sigma_{eq}}{2} = \left[ \left( \frac{\Delta\sigma}{2} \right)^2 + \left( \frac{\sqrt{3}\Delta\tau}{2} \right)^2 \right]^{1/2} \quad (3)$$

$$\frac{\Delta\varepsilon_{eq}}{2} = \left[ \left( \frac{\Delta\varepsilon}{2} \right)^2 + \left( \frac{\Delta\gamma/\sqrt{3}}{2} \right)^2 \right]^{1/2} \quad (4)$$

where  $\Delta\sigma$  and  $\Delta\tau$  are axial and torsional stress ranges, respectively, while  $\Delta\varepsilon$  and  $\Delta\gamma/2$  are axial and shear strain ranges.

In order to obtain a circular strain path, the components of strain are defined by the following expressions

$$\varepsilon = \frac{\Delta\varepsilon_{eq}}{2} \sin(\omega t); \quad \gamma = \sqrt{3} \frac{\Delta\varepsilon_{eq}}{2} \sin(\omega t + \pi/2) \quad (5)$$

## 4 Experimental Results and Their Discussion

### 4.1 Effects Observed During Cyclic Loading

Figure 3 shows in the stress plane the material responses to the strain controlled non-proportional cyclic loadings along circular path schematically presented in Figure 2a for all materials tested under the same total strain amplitude  $\Delta\epsilon_{eq}/2$  equal to 0.65%. Under these conditions the materials exhibits a hardening effect expressed by an increase of the stress amplitude. However, in the case of steel tested at a strain amplitude equal to 0.3% (range of small plastic strain) an opposite effect is observed, i.e. the effect of softening expressed by significant decrease of stress amplitude for the subsequent loading cycles. Such phenomenon is clearly visible in Figure 5, which presents diagrams illustrating variations of maximum values of axial and shear stress components versus the number of cycle.

The most remarkable hardening during cycling with a strain amplitude 0.65% is achieved for the aluminium alloy, Figure 3. A saturation cycle during cyclic loading is achieved for the brass (Figure 4) and steel (Figure 5). In the case of the aluminium alloy, Figure 6, a gradual stabilisation of the maximum values of stress components at subsequent cycles can be observed, however, the saturation cycle was not attained after 20 full cycles. For smaller magnitudes of strain amplitudes taken into account (0.15% for steel, 0.15% and 0.3% for aluminium alloy) both materials do not exhibit, practically, neither hardening nor softening effects (Figures 5 and 6). Such a situation is due to the fact that the just indicated strain amplitudes considered in the programme correspond to the elastic stress range.

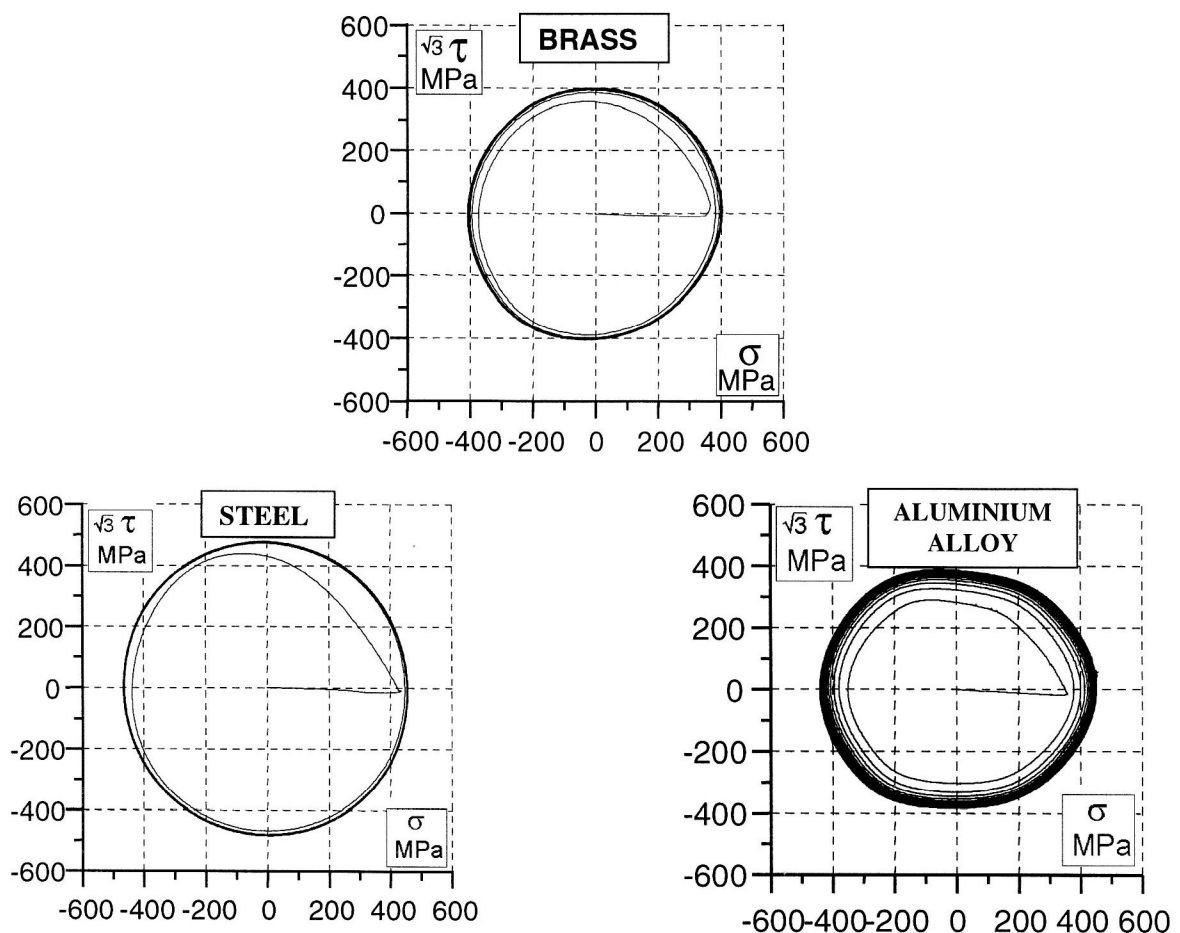


Figure 3. Stress Responses to the Total Strain Controlled Non-proportional Cycles along Circular Path with Strain Amplitude Equal to 0.65% for Brass, Steel, and Aluminium Alloy

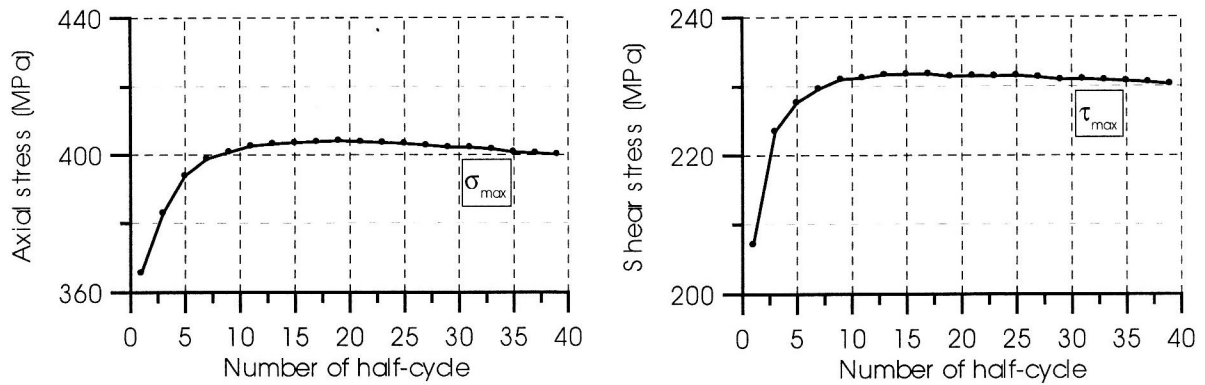


Figure 4. Maximum Peaks of Axial and Shear Stresses during Cyclic Loading of Brass along Circular Path (Total Strain Amplitude 0.65%, Frequency of Cycling 0.01Hz)

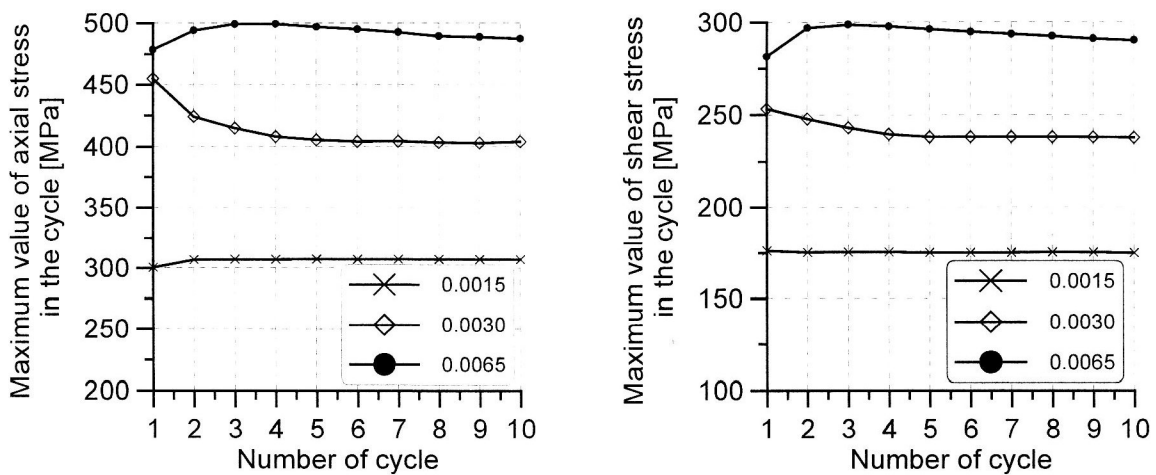


Figure 5. Maximum Peaks of Axial and Shear Stresses during Circular Cycles of Steel; Tests under Frequency of 0.025Hz. (The Numbers in the Labels Denote Magnitudes of the Total Strain Amplitudes)

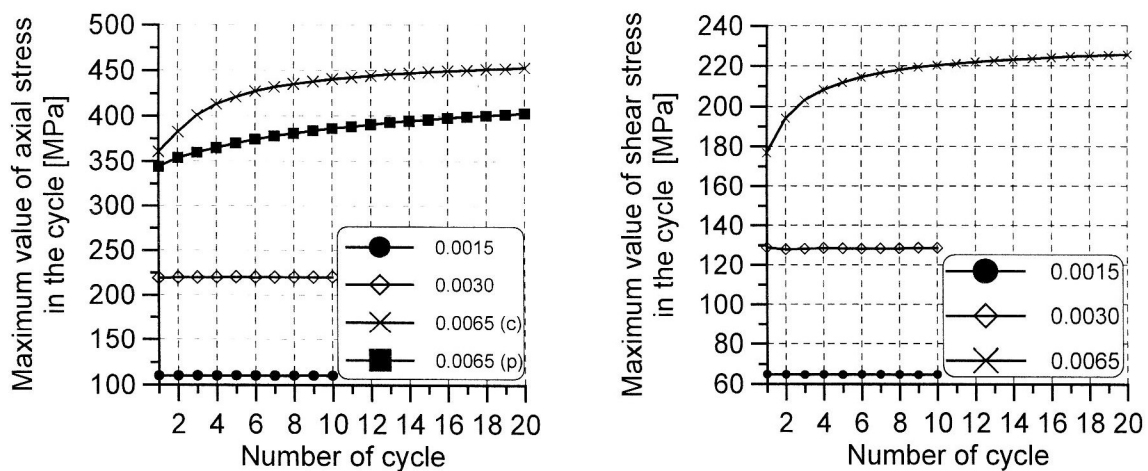


Figure 6. Maximum Peaks of Axial and Shear Stresses during Circular Cycles of Aluminium Alloy; Tests Carried Out under Frequency of 0.025Hz. The Numbers in the Labels Denote Magnitudes of the Total Strain Amplitudes Considered. (The Letters "c" and "p" are Used to Distinguish between the Circular and the Proportional Cyclic Loading Results for Strain Amplitude 0.0065)

In the diagram showing the variations of the maximum value of axial stress during subsequent cycles (Figure 6), besides of the data for the material tested under non-proportional loading, the results obtained under tension-compression cycling are presented for the strain amplitude equal to 0.65%. In order to distinguish the results obtained under the same strain amplitude, but using different types of cyclic loading, different symbols are used: square for the proportional loading, cross for the non-proportional cycles along circular path. Comparison of these results identifies clearly an additional hardening of the aluminium alloy observed for the non-proportional cyclic deformation.

A graphical presentation of the registered signals of strain and stress components as a function of time reveals remarkable phase shift between corresponding components of strain and stress. Typical examples of this phenomenon are shown in Figure 7 for axial and shear components obtained during investigation of brass (Figure 7a), 55 steel (Figure 7b), and PA6 aluminium alloy (Figure 7c). A difference between a time corresponding to the strain peak and that to the stress peak in a cycle defines the retardation time. This fact has not been sufficiently exposed in previous publications, and it seems that it can be responsible for an additional hardening/softening effect in metals undergoing to non-proportional loading in comparison to the hardening/softening usually observed for a proportional one.

It has to be emphasised that the phase shift between stress and strain components has not been observed for the tests on steel and aluminium alloy carried out under the proportional cycles. An example is presented in Figure 8 for proportional cycles along strain path related to the condition  $\epsilon = \gamma/2$ . A sinusoidal signal of strain was used to control the test in case of steel, while for aluminium alloy the triangular signal was applied. The phase shift has been neither observed during tests carried out under non-proportional cyclic loading, the level of which was within the range of the elastic stresses, Figure 9. On the basis of experimental data we can conclude that the phase shift effect depends of the type of loading and its magnitude, and therefore, it could be observed for non-proportional loading causing stresses higher than the yield point. From microscopical point of view, this means that it is associated with mechanisms of plastic deformations.

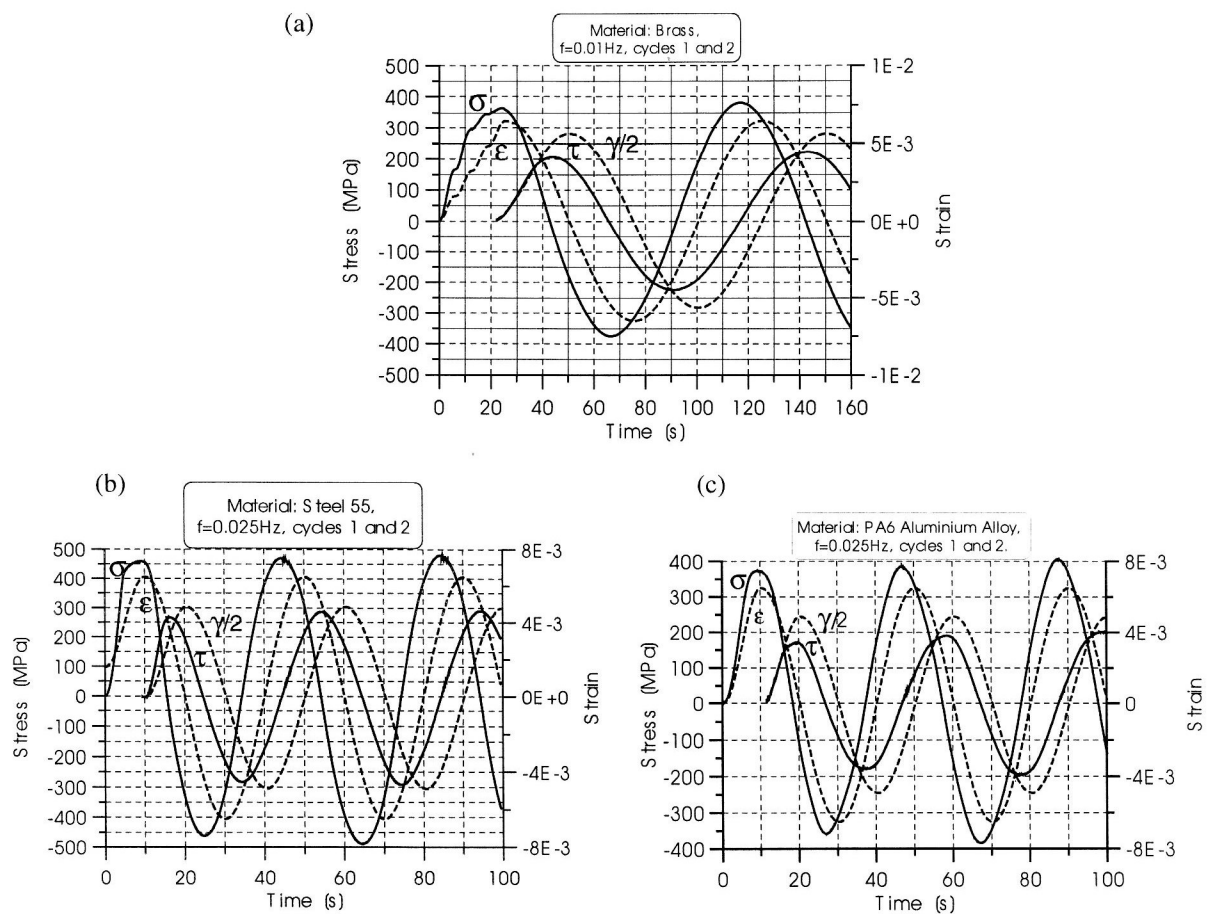


Figure 7. Retardation Time Observed during Non-proportional Loading of: (a) Brass, (b) Steel and (c) Aluminium Alloy

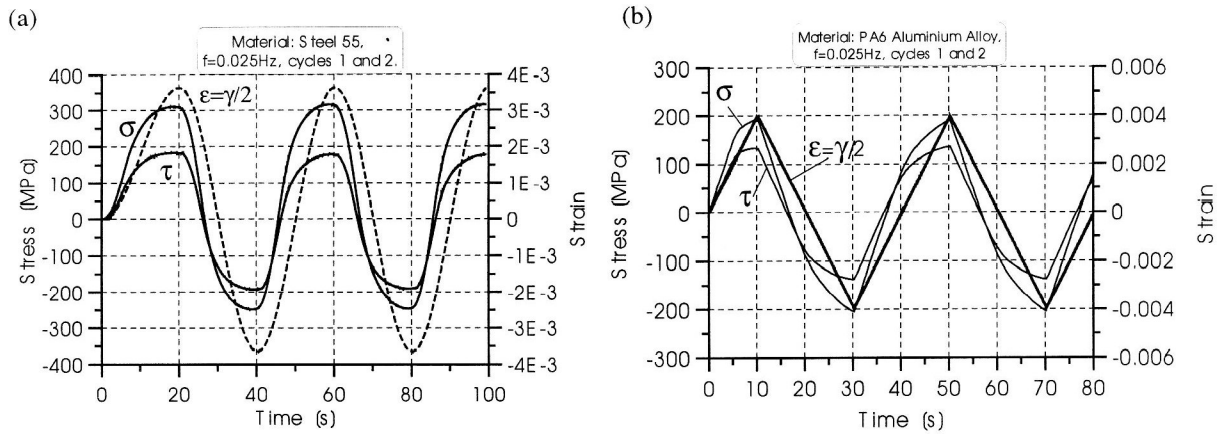


Figure 8. Variations of the Stress and Strain Components during Proportional Cyclic Loading for: (a) Steel (Strain-Controlled Signal in Form of Sinusoid), (b) Aluminium Alloy (Strain-Controlled Signal in Form of Triangle)

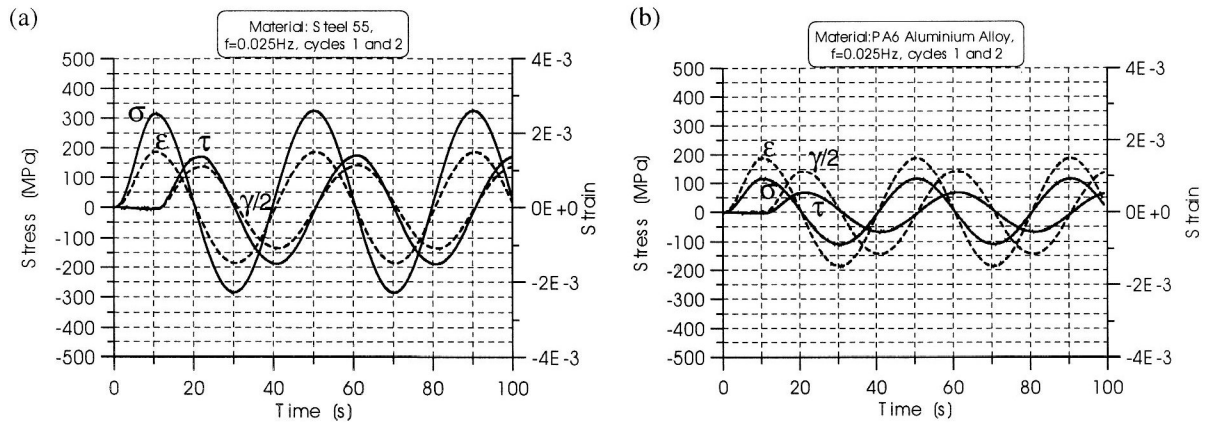


Figure 9. Variations of the Stress and Strain Components during Non-proportional Cyclic Loading Carried Out under Elastic Stress Level for: (a) Steel, (b) Aluminium Alloy

On the other hand, a coincidence of the maximum levels of strain and stress in a single cycle during the proportional loading is presumably caused by a lack of the principal stresses rotation. Thus, it seems reasonable to relate its existence under circular loading cycles, covering the plastic range of deformation, to the rotation of principal stresses directions, typical for this kind of loading.

The experimental programme performed for a range of strain amplitudes and frequencies allowed clear observation of an effect of the strain-rate on material behaviour. To evaluate it, the stress-strain loops for both axial and shear components have been analysed carefully together with time variations of appropriate stress and strain components. As a consequence, the retardation time between strain and stress for both components has been determined. Having this parameter, and data concerning time of loading cycle, the retardation angle has been calculated for all strain rates and amplitudes. A procedure for determination of a value of retardation angle is quite simple. In order to obtain such value in a single cycle it is sufficient to consider functions of the strain and stress signals, which are defined in the following form

$$\begin{aligned} \sigma &= \sigma_a \sin(\omega t) \\ \varepsilon &= \varepsilon_a \sin(\omega[t - t_0]) \end{aligned} \quad (6)$$

where  $\omega$  denotes angular rate,  $\sigma_a$  and  $\varepsilon_a$  are the maximum stress and maximum strain amplitudes, respectively,  $t$  denotes current time, and  $t_0$  is the retardation time between stress and strain peaks obtained from experimental data.

If  $\omega t = \pi/2$ , then the expressions defined in equation (6) take the form

$$\sigma = \sigma_a$$

$$\varepsilon = \varepsilon_a \sin\left(\frac{\pi}{2} - \omega t_0\right) = \varepsilon_a \cos(\omega t_0) \quad (7)$$

Simple transformation of equation (7) leads to the following expressions

$$\frac{\sigma}{\sigma_a} = 1$$

$$\frac{\varepsilon}{\varepsilon_a} = \cos(\omega t_0) = \cos(\delta) \quad (8)$$

which allow to calculate a retardation angle between stress and strain in the arbitrarily chosen single cycle. Variations of this parameter are presented in Figure 10a as a function of the number of strain half-cycle in the case of brass, and as a function of cyclic frequency in the case of steel (Figure 10b) and aluminium alloy (Figure 11c). It is easy to note that the retardation angle depends strongly on the magnitude of the strain amplitude. It grows with the increase of the strain amplitude. Moreover, it can be seen that if the total strain amplitude has a magnitude which corresponds to the elastic stress level, then the retardation angle takes a very small value (see data for steel, Figure 10b) or vanishes (see data for aluminium alloy, Figure 10c). The results in Figures 10b and 10c indicate that a frequency of cyclic loading also may have an influence on the retardation angle. However, the sensitivity of this parameter is much weaker than the strain amplitude variations. On the basis of the diagrams presented in Figure 10 it can be concluded that the value of retardation angle is dependent on the strain amplitude and frequency of cycling, and as a consequence, on the strain-rate. Therefore, in order to elaborate rational constitutive relationships such effects should be taken into account by researchers modelling behaviour of metallic materials working under non-proportional loading.

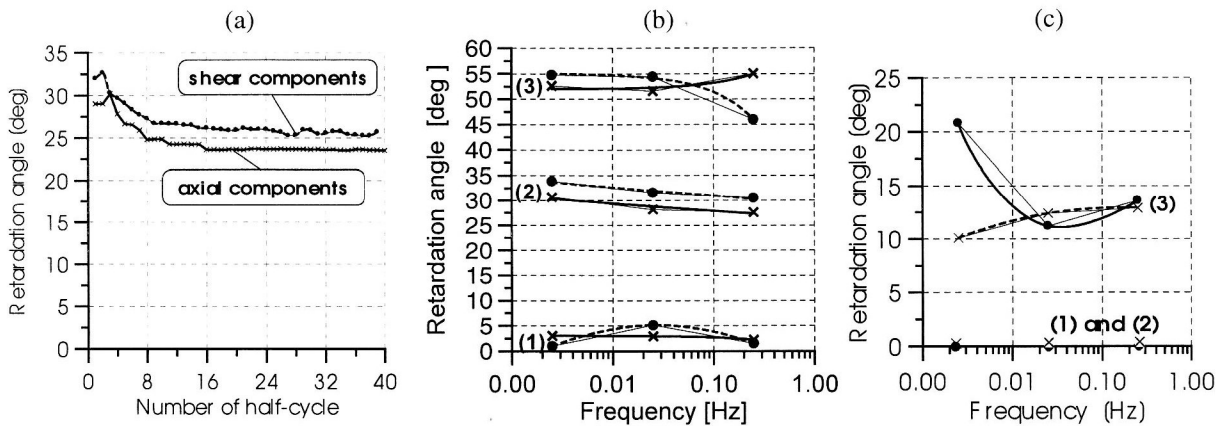


Figure 10. Variations of Retardation Angle: (a) the Results for Brass Tested under Cyclic Loading with Strain Amplitude 0.65%, (b) the Results for Steel Tested under Cyclic Loading with Three Strain Amplitudes (1) - 0.15%; (2) - 0.3%; (3) - 0.65%, (c) the Results for Aluminium Alloy Tested under Cyclic Loading with Three Strain Amplitudes (1) - 0.15%; (2) - 0.3%; (3) - 0.65%. (Solid Lines in Diagrams (b) and (c) Denote Retardation Angle Variations for Axial Components, Broken Lines for Shear Components).

The results obtained for all tested materials also allow to assess the phase shift between stress and plastic strain rate. In order to determine this parameter it is necessary to calculate the components of plastic strain rate. The representative results are shown in Figure 11 for aluminium alloy and steel investigated at the strain amplitude equal to 0.65% and frequency of cyclic loading 0.025Hz. In both cases plastic strain components are presented at points where the maximum values of stress components were achieved. At each of these points the axial and shear components of the plastic strain rate and their resultant are plotted. It enables to identify in a simple way effect of non-co-axiality of stress and plastic strain rate. The diagrams presented in Figure 11 also allow to evaluate an evolution of this effect due to magnitude variation of the stress components. As a consequence, an influence of strain-induced anisotropy on the rate-type constitutive equation of plasticity can be analysed.

Comparison of the stress and plastic strain rate components, calculated on the basis of strain variations during tests, shows again a marked phase shift effect. Such shift depends on the strain amplitude and frequency of cycling in the same way as the phase shift between maximum values of stress and total strain. It has to be emphasised that the magnitudes of both these shifts are not the same, however, their character of variation is quite similar.

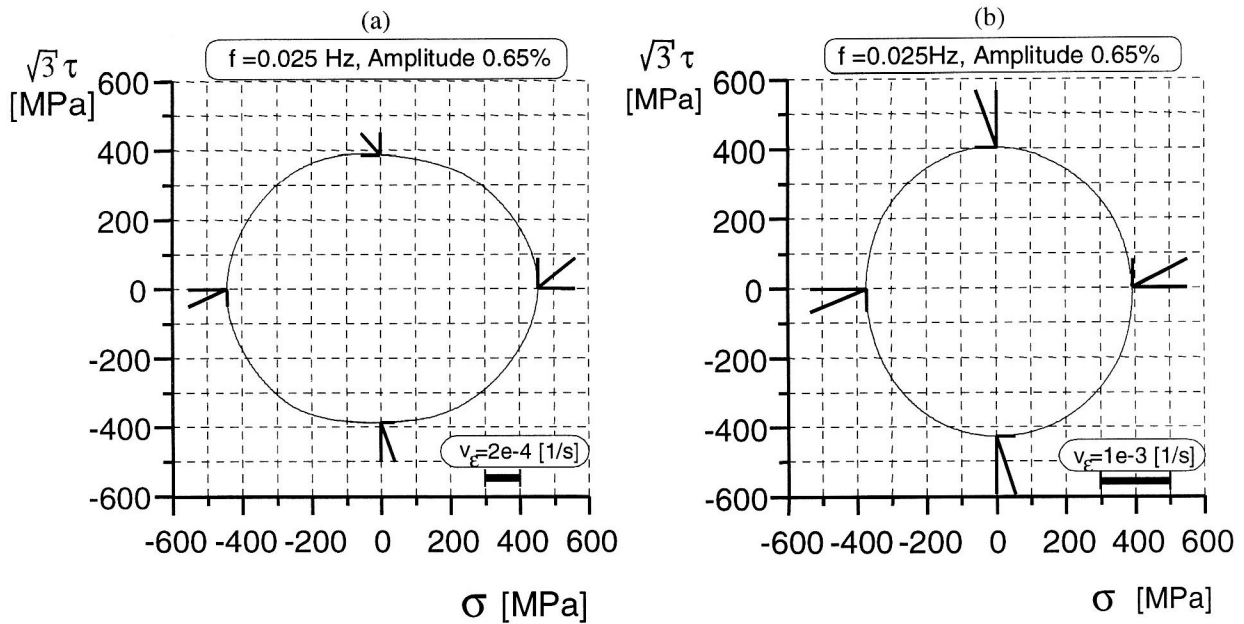


Figure 11. Stress Variations at 9th Circular Cycle and Strain Rate Components for Maximum Stress Components : (a) Aluminium Alloy, (b) Steel.

#### 4.2 Effects Observed After Cyclic Loading

The second part of the experimental programme is devoted to the evaluation of the influence of prior deformation induced by means of cyclic loading on the mechanical properties of the tested materials. An analysis of mechanical properties variations due to cyclic loading is based on the yield surface concept. In the first step a preliminary yield surface for each material has been determined for the offset strain equal to 0.005%. The surfaces were determined using the single-specimen method (Kowalewski and Śliwowski, 1997, Kowalewski, 1997). An initial yield surface has been determined for each material tested in order to identify an initial anisotropy. All materials tested in the as-received state exhibit certain anisotropy, which can be clearly identified by comparison of the ratio of yield surface main axes with that resulting from the isotropic Huber-v. Mises yield condition (1.73). In the case of aluminium alloy a flattening of the yield surface in comparison to that resulting from the isotropic Huber-v. Mises yield condition reflects an initial anisotropy. The ratio of the major and minor yield surface axes takes the value equal to 1.95. The 55 steel and MO58 brass also exhibit anisotropic behaviour in the as-received state. In these cases, however, the effect manifests itself by the shift of yield locus in the compression direction (brass) or torsion direction (steel).

In order to analyse the effects of prestraining all materials tested were predeformed using non-proportional cyclic loading along circular strain path. For aluminium alloy and steel also proportional cyclic loading was applied in order to identify a difference in material response in comparison to non-proportional loading having the same strain amplitude. Plastic property variations are analysed on the basis of the initial yield surface evolution. The representative results are shown in Figures 12 and 13. Considerations of the three kinds of metallic materials after prestraining have shown that mechanical properties for all of them undergo significant variations in the strain range taken into account. Yield surfaces presented in Figures 12 and 13 correspond to the same offset strain equal to 0.005%. The brass exhibits a kinematic hardening effect expressed by the shift of the subsequent yield locus with respect to the location of the initial yield locus, Figure 12. For the aluminium alloy also a hardening effect was observed. However, in this case it has more complicated character. Besides of the kinematic hardening the material exhibits isotropic hardening expressed by the remarkable increase of the subsequent yield locus dimensions in comparison to the initial ones, Figure 13.

The hardening effect of both materials is directly connected with the loading history and can be simply interpreted by an analysis of the stress response to the strain controlled cyclic prestraining. The materials during cyclic loading carried out with constant strain amplitude experienced the hardening effect expressed by the difference between the saturation loop and the stress hysteresis loop obtained in the first cycle, Figure 3. Such hardening effect is responsible for an increase of the yield surface sizes for the cyclically prestrained materials. An opposite effect after prestraining is observed for the steel. An analysis of the shapes and sizes of the yield loci for steel implies the principal conclusion that the prior deformation induced during cyclic loading caused softening effect expressed by the significant shrinkage of the subsequent yield locus with respect to the initial yield surface, Figure 13. It has to be noted that in this case it is difficult to explain this property on the basis of diagrams representing the stress response to strain-controlled cyclic deformation. In spite of the cyclic hardening observed for the highest strain amplitude cycles, Figure 3, the steel exhibits the softening effect after cyclic prestraining, Figure 13.

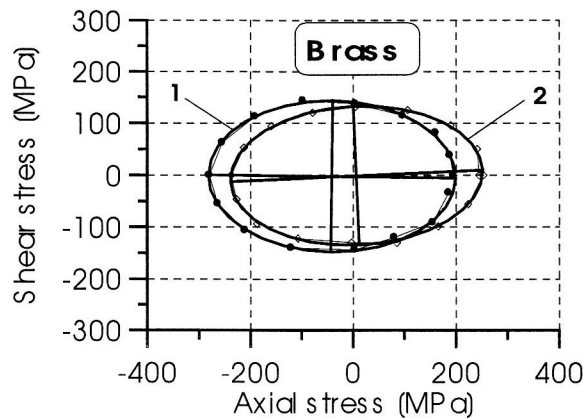


Figure 12. Evolution of the Yield Surface Positions and Sizes due to Cyclic Loading of Brass. The Numbers 1, 2 in Diagrams Denote, respectively, Initial Yield Locus, Subsequent Yield Locus after Non-proportional Loading with Strain Amplitude Equal to 0.65%.

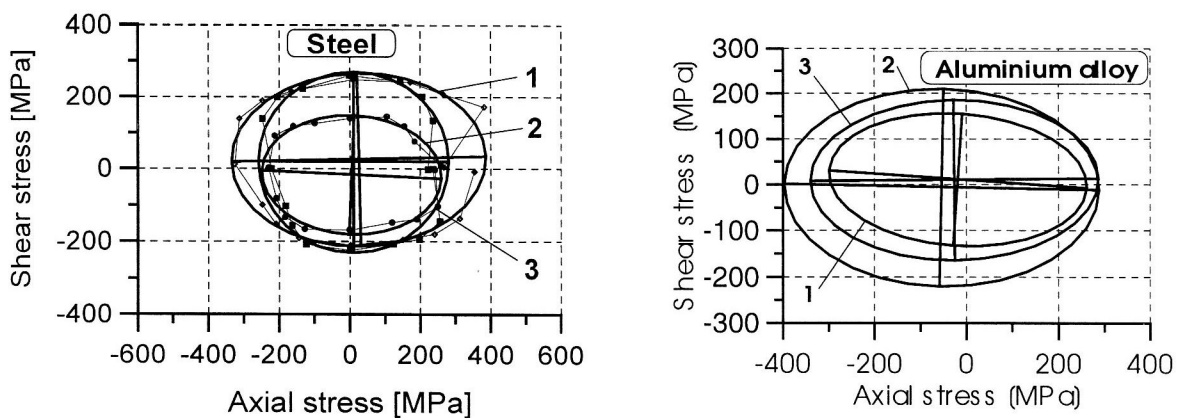


Figure 13. Evolution of the Yield Surface Positions and Sizes due to Cyclic Loading of Steel and Aluminium Alloy. The Numbers 1, 2 and 3 in Diagrams Denote, respectively, Initial Yield Locus, Subsequent Yield Locus after Non-proportional Loading with Strain Amplitude Equal to 0.65%, Subsequent Yield Locus after Proportional Cyclic Loading (Tension - Compression) with Strain Amplitude Equal to 0.65%.

In the diagrams representing the results for steel and aluminium alloy, besides of the initial yield surface and subsequent yield locus of the material after non-proportional loading, the yield surface after proportional tension-compression cyclic loading is presented. The aluminium alloy after this kind of loading exhibits an isotropic hardening. An opposite effect is achieved for the steel. Comparison of the yield loci after two different types of

cyclic loading identifies, in the case of aluminium alloy, an effect of the additional hardening associated with the non-proportional cyclic loading. The same comparison for the steel reveals the additional softening.

## 5 Conclusions

Multiaxial cyclic behaviour of three metallic materials has been investigated experimentally. For this purpose, two kinds of cyclic tests were carried out for uniaxial tension-compression cycle and the multiaxial non-proportional circular cycle. The main conclusions stemming from this research can be summarised as follows

- The results for steel achieved under three levels of strain amplitude of non-proportional cyclic loading discover the important fact from engineering point of view, namely, an appearance of hardening or softening depends on the loading amplitude.
- Independently of the material, the results recorded during the non-proportional tests exhibited a significant effect of a phase shift of maximum strain with respect to the corresponding maximum stress, which has not been observed during proportional loading. A magnitude of this shift depends on the material, and for the selected material on the strain amplitude and frequency of cyclic loading.
- An influence of prior cyclic loading on mechanical properties of the materials has been studied on the basis of an initial yield surface evolution. The brass and aluminium alloy exhibited hardening due to cyclic loading, while for the steel a softening effect was observed in the strain range taken into account.

## Acknowledgement

The support from the Polish State Committee for Scientific Research under grant 7T07A 00218 is gratefully acknowledged.

## Literature

1. Benallal, A., Marquis, M.: Constitutive equations for non-proportional cyclic elasto-viscoplasticity, *ASME J. Eng. Mat. Tech.*, 109, (1987), 326-335.
2. Cailletaud, G., Doquet, V., Pineau, A.: *Cyclic multiaxial behavior of an austenitic stainless steel, Fatigue under Biaxial and Multiaxial Loadings*, 131-149, London: Mechanical Engineering Publications (1991).
3. Calloch, S., Marquis, D.: Additional hardening due to tension-torsion non-proportional loadings: Influence of the loading path shape, *Multiaxial Fatigue and Deformation Testing Techniques*, ASTM STP 1280, Philadelphia, (1997), 113-130.
4. Cheng, S., Krempl, E.: Experimental determination of strain-induced anisotropy during non-proportional straining of an Al/Mg alloy at room temperature, *Int. J. Plasticity*, 7, (1991), 827-846.
5. Dietrich, L., Kowalewski Z.L., Experimental investigation of an anisotropy in copper subjected to predeformation due to constant and monotonic loadings. *Int. J. Plasticity*, 13, (1997), 87-109.
6. Dietrich, L., Socha, G., Kowalewski, Z.L.: Influence of loading parameters on behaviour of 55 steel under complex stress states due to circular strain path, *Proc. 19<sup>th</sup> Symp. Exp. Mech. of Sol.*, Jachranka (2000), ZGPW, Warsaw, (2000), 556.
7. Doong, S.H., Socie, D.F.: Deformations mechanisms of metals under complex non-proportional cyclic loading, *Fatigue under Biaxial and Multiaxial Loadings*, pages 305-320, London: Mechanical Engineering Publications (1991).
8. Khan, A.S., Wang, X.: On non-proportional infinitesimal plastic deformation after finite plastic prestraining and partial unloading, *J. Mech. Phys. Solids*, 36, (1988), 519-535.
9. Kowalewski, Z.L.: Assessment of cyclic properties of 18G2A low-alloy steel at biaxial stress state, *Acta Mech.*, 120, (1997), 71-89.
10. Kowalewski, Z.L., Śliwowski, M.: Effect of cyclic loading on the yield surface evolution of 18G2A low-alloy steel, *Int. J. Mech. Sci.*, 39, (1997), 51-68.
11. Krempl, E., Cheng S., The experimental determination of the stress responses of an Al/Mg alloy to a polygonal strain path after three levels of prestraining, *Acta Mechanica* 101, (1993), 93-109.
12. Krempl, E., Lu, H.: The hardening and rate-dependent behavior of fully annealed AISI type 304 stainless steel under biaxial in-phase and out-of-phase strain cycling at room temperature, *Trans. ASME J. Eng. Mat. Tech.*, 106, (1984), 376-382.
13. Lamba, H.S., Sidebottom, O.M.: Cyclic plasticity for non-proportional paths, *ASME J. Eng. Mat. Tech.*, 100, (1978), 96-111.

14. Murakami, S., Kawai, M., Aoki, K., Ohmi, Y.: Temperature-dependence of multiaxial non-proportional cyclic behavior of type 316 stainless steel, *ASME J. Eng. Mat. Tech.*, 111, (1989), 32-39.
15. Murakami, S., Kawai, M., Ohmi, Y.: Effects of amplitude-history and temperature-history on multiaxial cyclic behavior of type 316 stainless steel, *ASME J. Eng. Mat. Tech.*, 111, (1989), 278-285.
16. Ohashi, Y., Kawai, M., Kaito, T.: Inelastic behavior of type 316 stainless steel under multiaxial non-proportional cyclic stressing at elevated temperature, *ASME J. Eng. Mat. Tech.*, 107, (1985), 101-109.
17. Tanaka, E.: A non-proportionality parameter and a cyclic viscoplastic constitutive model taking into account amplitude dependences and memory effects of isotropic hardening, *European Journal of Mechanics, A/Solids*, 13, (1994), 155-173.

---

*Address:* Prof. Zbigniew Kowalewski, Institute of Fundamental Technological Research, Polish Academy of Sciences 00-049 Warsaw, ul. Świętokrzyska 21, Poland, E-mail: zkowalew@ippt.gov.pl